








Research Article

Effect of Viscosity on Stopping Power for a Charged Particle Moving above Two-Dimensional Electron Gas

Lei Chen ¹, Yu Wang ², Yuesong Jia,³ Xianjun Yang,⁴ Chunzhi Li,⁵ Lin Yi ¹,
Wei Jiang ¹ and Ya Zhang ²

¹School of Physics, Huazhong University of Science and Technology, Wuhan 430074, China

²Department of Physics, Wuhan University of Technology, Wuhan 430070, China

³Institute of Fluid Physics, China Academy of Engineering Physics, Mianyang 621900, China

⁴Institute of Applied Physics and Computational Mathematics, Beijing 100094, China

⁵College of Mathematics and Physics, Inner Mongolia University for the Nationalities, Tongliao 028043, China

Correspondence should be addressed to Wei Jiang; weijiang@hust.edu.cn and Ya Zhang; zhangya.jiayou@gmail.com

Received 2 December 2021; Accepted 4 April 2022; Published 29 April 2022

Academic Editor: Dieter H.H. Hoffmann

Copyright © 2022 Lei Chen et al. This is an open access article distributed under the Creative Commons Attribution License, which permits unrestricted use, distribution, and reproduction in any medium, provided the original work is properly cited.

In two-dimensional (2D) electron systems, the viscous flow is dominant when electron-electron collisions occur more frequently than the impurity or phonon scattering. In this work, a quantum hydrodynamic model, considering viscosity, is proposed to investigate the interaction of a charged particle moving above the two-dimensional viscous electron gas. The stopping power, perturbed electron gas density, and the spatial distribution of the velocity vector field have been theoretically analyzed and numerically calculated. The calculation results show that viscosity affects the spatial distribution and amplitude of the velocity field. The stopping power, which is an essential quantity for describing the interactions of ions with the 2D electron gas, is calculated, indicating that the incident particle will suffer less energy loss due to the weakening of the dynamic electron polarization and induced electric field in 2D electron gas with the viscosity. The values of the stopping power may be more accurate after considering the effect of viscosity. Our results may open up new possibilities to control the interaction of ions with 2D electron gas in the surface of metal or semiconductor heterostructure by variation of the viscosity.

1. Introduction

The interaction of charged particles with matter is an essential issue for a variety of physical systems, which has been a subject of extensive research since the discovery of subatomic particles [1]. Especially, the interests in surface physics are at the focus of much current research on charged particles interacting with two-dimensional (2D) electron gases [2–5]. Most intriguing is perhaps energy loss, i.e., so-called stopping power and the perturbed electron gas density induced by the charged particle in the interaction process [6–9]. Studying the stopping power of charged particle in dense plasmas is crucial for applications in high energy density physics [10, 11] and fundamental plasma physics [7, 12, 13], which can help us to make an accurate understanding of ion beam transport. Additionally, in ion beam

analysis, where the stopping power of detected projectiles is the common observable quantity, the specific stopping power can obtain accurate depth perception [14]. Furthermore, the information given by the energy loss process in plasma is crucial for characterization and surface modification schemes [15–17] of the 2D system using projectiles in the matter as a powerful tool.

Stopping power is a measure of the ability of a material to slow down energetic particles that travel above the 2D sheet and 3D bulk [18]. When a charged particle moves with constant velocity near to a 2D sheet, the charged particle loses its kinetic energy, and the electron gas density of the 2D sheet is perturbed due to ionization and excitation of the electrons [19]. The stopping power, i.e., the energy lost per unit path length, is a substantial quantity used to predict and understand the effects of particle radiation in the matter, ion

ranges, and the energy deposited [20–22]. There have been many works, both theoretical and experimental, investigating the stopping power [23–27]. Horing first investigated the energy loss of the fast particle moving parallel to the two-dimensional plasma sheet with a fixed distance by using the random-phase approximation (RPA) theory [28]. Apart from RPA theory, much work was carried out to study the stopping power by using the dielectric and binary collision theories [29–31], the quantum scattering theory [32], and the local field correction (LFC) [33, 34]. In addition, the density functional theory [35, 36], the first principles [18], and the particle-in-cell (PIC) and molecular dynamics (MD) [19, 37–38] were also adopted to study the interaction process between the ions and plasma. Recently, some progress has been made in the experimental study of the stopping power. J. Ren and coworkers [11] have performed an experiment to demonstrate the existence of collective effects, for high-density beam, leading to enhanced stopping. Their results play an important role in the optimum design of ion-driven inertial confinement fusion and fast ignition schemes. The importance of excited projectile states has been reported by Y. Zhao et al. [13] in the stopping process, providing significant support for the relevant research like the atomic process in the solar wind.

So far, with technological development in the area of miniaturized devices and the advances in nanofabrication techniques, plasmonic materials containing fully degenerated electrons have recently received renewed attention [39–42]. The quantum mechanical effects for the theoretical description of quantum plasma must be taken into account. For accurately understanding the dynamics of 2D quantum electron gas, the use of the quantum hydrodynamic model (QHD) is required, which was developed by solving the nonlinear Schrödinger–Poisson or the Wigner–Poisson kinetic models [43, 44]. Also, based on this model, both the quantum statistical and quantum diffraction effects have been proved to play an essential role in studying the interactions of charged particles with the quantum electron gas [45–48].

Interactions between particles in quantum many-body systems can bring about the collective behavior described by hydrodynamics. Some new features in the two-dimensional electron gas of the hydrodynamic regime will be produced on the condition that the typical length scale of electron-electron scattering (l_{ee}) is shorter than those of electron-disorder and electron-phonon scatterings (l), i.e., $l_{ee} \ll l$. Under these conditions, the electrons show the trend of collective motion, and the electron transport is dominated by the viscosity [49]. In other words, in materials in which electrons strongly interact with each other or with phonons, electron transport is thought to be similar to viscous flows [50]. Furthermore, when electron-electron collisions occur more frequently than the impurity or phonon scattering, the viscous current is expected to be dominant [51]. For example, in graphene, which hosts a unique electron system, the electron-phonon scattering is extremely weak, but electron-electron collisions are sufficiently frequent to provide the local equilibrium above the temperature of liquid nitrogen. In this instance, the electrons can behave as

a viscous flow and exhibit hydrodynamic phenomena similar to classical flows [52].

Recently, experiments on WP_2 [50, 51] and $GaAs$ have many features demonstrating the viscous flow of electrons. The shear forces caused by the viscosity at the channel walls result in a nonuniform velocity profile, so that the electrical resistivity becomes a function of the channel width, suggesting a viscosity-induced dependence of the electrical resistivity on the sample width [50]. Moreover, compared with the Ohmic flow of the particles in a mesoscopic two-dimensional electron gas in a $GaAs$ quantum well in the hydrodynamic regime [51], the viscosity can cause backflow of the current and negative nonlocal voltage. In addition, the experimental results of Gusev G et al. confirm the theoretically predicted significance of viscous flow in mesoscopic two-dimensional electron gas [53]. Then, they studied experimentally an electronic analog of the Stokes flow around a disc immersed in a two-dimensional viscous liquid of the $GaAs$ quantum wells. The results confirm theoretical predictions and open up the possibility of controlling the current in the microstructure by changing the viscosity [54]. Moreover, a series of updated theoretical approaches have been published [55–58] considering a viscous system. Meanwhile, the viscous quantum hydrodynamic model has been used for many studies, such as the quantum semiconductor devices [59–61], nonlinear plasma oscillations [62] and the Jeans self-gravitational instability for dense quantum viscous plasma [63].

However, to the best of our knowledge, viscosity in the two-dimensional quantum electron gas (2DQEG) effect has not been considered in beam-2DQEG interactions. Thus, an interesting question arises: How is the strength of the stopping power changed in the viscous 2D quantum electron gases? In this work, the main aim is to study the interaction between charged particles and 2D quantum electron gases in viscosity. We propose a revised quantum hydrodynamic model for a viscous two-dimensional quantum electron based on the model obtained in reference [64]. The outline of the study is as follows. In Section 2, we introduce our quantum hydrodynamic model and then derive the analytical expressions of the stopping power, the perturbed density, and the velocity vector field of perturbed electron gas based on revised QHD. In Section 3, numerical results of the perturbed density, spatial distribution of the velocity field, and the stopping power are discussed in different conditions. Moreover, we present the viscosity impacts on these quantities. Finally, a summary is given in Section 4. Gauss units will be adopted throughout the study.

2. Quantum Hydrodynamic Model

2.1. The Viscosity Coefficient. In the hydrodynamic regime, electronic dynamics is dominated by viscosity, rather than impurity scattering [56]. The electron flow in which numerous target nuclei are suspended (forming a suspension-like) may be regarded as a homogeneous medium. Such a medium has an effective viscosity η [65]. In the present work, we neglect the compressibility, the thermal conductivity effects, and magnetic and temperature effects. Viscosity is solely

characterized by momentum relaxation in fluid. It should be noted that in general, the electron viscosity is not necessarily related to electron-electron collisions. Any process providing the relaxation of the second moment of the electron distribution function leads to viscosity. Thus, the viscosity coefficient η is proportional to the second-order relaxation time τ_2 [55].

$$\eta = \frac{1}{4}v_F^2\tau_2, \quad (1)$$

$$\frac{1}{\tau_2(T)} = \frac{1}{\tau_{2,ee}(T)} + \frac{1}{\tau_{2,0}},$$

where v_F is the Fermi velocity. Additionally, $1/\tau_{2,ee}(T)$ is the interelectron relaxation rate, while $1/\tau_{2,0}$, being the ‘‘residual’’ relaxation rate of the shear stress at $T \rightarrow 0$ owing to scattering of electrons on disorder, is not related to the electron-electron collisions [55, 66]. The temperature effect is not considered here, i.e., $\tau_2 \approx \tau_{2,0}$. Furthermore, the character of the viscous flow strongly depends on the geometry and probe configurations of the sample in general. For instance, the velocity field in a curved pipe flow becomes more nonuniform than in a straight pipe, which may enhance the viscosity effect [53]. In principle, a range of viscosity values is to be expected in different electron flows [67]. For a typical system of the viscous flow, the high-quality *GaAs* quantum wells with the electron density $n \approx 9.1 \times 10^{11} \text{cm}^{-2}$, $2.9 \times 10^{11} \text{cm}^{-2}$, or $6.0 \times 10^{11} \text{cm}^{-2}$, the following fitting parameters, $\tau_{2,0} = 0.8 \times 10^{-11} \text{s}$, $1.1 \times 10^{-11} \text{s}$, or $0.69 \times 10^{-11} \text{s}$, are used in references [51, 53, 55]. The viscosity coefficient η values of two well-known 2D electron flows, *GaAs* quantum wells at 1.4 K of two different configurations and graphene, are $1200 \text{cm}^2 \text{s}^{-1}$, $3000 \text{cm}^2 \text{s}^{-1}$, and $1000 \text{cm}^2 \text{s}^{-1}$ [51–53], respectively, an order of magnitude higher than that of honey. For comparison, liquid honey has typical viscosities of $20\text{--}50 \text{cm}^2 \text{s}^{-1}$ [52]. The τ_2 is related to the temperature and density of the material. $r_s = (2\pi n_0 a_B^2)^{-1/2}$ is also the function of density dependent on the material character. Therefore, when the temperature takes a certain value, the value of τ_2 for the corresponding range can be obtained by giving the value of the density function r_s , as reported in [66].

Consequently, as for $r_s = 2$, we can set the values of $\tau_{2,0}$ in the range between $\tau_2 \approx \tau_{2,0} = 1.1 \times 10^{-16} \text{s}$ and $1.1 \times 10^{-13} \text{s}$ at $T \rightarrow 0$, since the characteristic time (inverse of the electron plasma frequency $1/\omega_p = (2\pi n_0 e^2/m_e a_B)^{-1/2}$) is about $10^{-16} - 10^{-13} \text{s}$. According to reference [66], the shear stress relaxation rate $1/\tau_2$ as the function of temperature for the *GaAs* quantum well was presented for the density $n = 1.6 \times 10^{11} \text{cm}^{-2}$, which increases from the order of 10^{11}s^{-1} to 10^{12}s^{-1} with increasing temperature T . Therefore, as for τ_2 , the order of 10^{-13}s – 10^{-16}s can be related with the graphene, GaN, and thin metal film for corresponding carrier concentrations n of the order of 10^{12}cm^{-2} , 10^{13}cm^{-2} , and $10^{12}\text{--}10^{16} \text{cm}^{-2}$ [47, 52, 68], the carrier concentrations of which can be changed by doping and other methods.

As a result, the corresponding viscosity η in the case assumed by this work can take values of $0.33 \text{cm}^2 \text{s}^{-1}$,

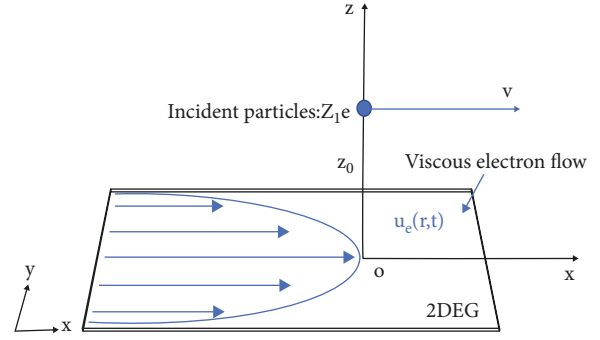


FIGURE 1: Schematic illustration of the interaction system: a particle of charge $Z_1 e$ moving with v above 2DEG described in Cartesian coordinate, $R = \{x, y, z\}$, along the x axis at a distance z_0 above the 2DEG plane.

$3.3 \text{cm}^2 \text{s}^{-1}$, $33 \text{cm}^2 \text{s}^{-1}$, and $330 \text{cm}^2 \text{s}^{-1}$. As follows, the influence of the viscous effect (1) is considered for the modified expressions of the perturbed density, the stopping power, and the velocity vector field of the perturbed electron gas.

2.2. Derivation of the Fluid Model. We consider an idealized 2DEG with an equilibrium density, $n_0 = n_{i0} = n_{e0}$, which is composed of free electrons and motionless ions. The region $z > 0$ is the vacuum. A particle of charge $Z_1 e$ moves with constant velocity v parallel to 2DEG along the x axis with density $\rho_{\text{ext}} = Z_1 e \delta(\mathbf{r} - \mathbf{v}t) \delta(z - z_0)$, where $\mathbf{v} = v \mathbf{e}_x$, $\mathbf{r} = \mathbf{r}(x, y)$, and z_0 is the distance from the plane, described in a Cartesian coordinate system with $R = \{x, y, z\}$, as shown in Figure 1. Therefore, the homogeneous 2DEG will be perturbed by the charged particle and can be regarded as a charged viscous fluid with velocity field $\mathbf{u}_e(\mathbf{r}, t)$ and the electron gas density (per unit area) $n_e(\mathbf{r}, t)$.

By employing the linearized quantum hydrodynamic model of the incompressible viscous fluid, the electronic excitation on the 2DEG surface can be described by the continuity equation as

$$\frac{\partial n_e}{\partial t} + \nabla_{\parallel} \cdot (n_e \mathbf{u}_e) = 0, \quad (2)$$

the momentum-balance equation as

$$m_e \left(\frac{\partial \mathbf{u}_e}{\partial t} + (\mathbf{u}_e \cdot \nabla_{\parallel}) \mathbf{u}_e \right) = e \nabla_{\parallel} \Phi|_{z=0} - \nabla_{\parallel} w_e + \frac{\hbar^2}{2m_e} \nabla_{\parallel} \left(\frac{1}{\sqrt{n_e}} \nabla_{\parallel}^2 \sqrt{n_e} \right) - \gamma m_e \mathbf{u}_e + m_e \eta \Delta_{\parallel} \mathbf{u}_e, \quad (3)$$

and Poisson’s equation as

$$\nabla^2 \Phi = 4\pi e [n_e \delta(z) - n_0 \delta(z) - Z_1 \delta(\mathbf{r} - \mathbf{v}t) \delta(z - z_0)], \quad (4)$$

where m_e is the electron mass, e is the elementary charge, and \hbar is the Planck constant divided by 2π . It is worth noting that, in (2) and (3), $\nabla_{\parallel} = (\partial/\partial x) \mathbf{e}_x + (\partial/\partial y) \mathbf{e}_y$, which is used to describe the quantum electron gas surface, is different from $\nabla = (\partial/\partial x) \mathbf{e}_x + (\partial/\partial y) \mathbf{e}_y + (\partial/\partial z) \mathbf{e}_z$ unrestricted in (4) and $\Delta_{\parallel} = \nabla_{\parallel}^2 = ((\partial^2/\partial x^2) + (\partial^2/\partial y^2))$. In addition, the

viscosity is taken into account through the coefficient of viscosity η . Φ is the total potential which consisted of the external potential Φ_0 of the moving charged particle and the induced potential, Φ_{ind} , generated by the perturbation of the electron gas density on the 2DEG surface. In the right-hand side of (3), the first term is the force on electrons of the electron gas surface given by the tangential component of the electric field. The second and third terms are regarded as the quantum effects due to the internal interactions in the electron species and the quantum pressure, where $w_e = \pi\hbar^2 n_e/m_e$, being the Fermi energy of 2DEG. The fourth term is the frictional force on electrons, owing to the positive charge background, with γ being the frictional coefficient, while the last term, $m_e\eta\Delta_{\parallel}\mathbf{u}_e$, is the viscous force result from the electron gas at different speeds, where η is the viscosity coefficient.

There is a weak perturbation in 2DEG by the moving charged particles. Hence, we can linearize the above equations by assuming the density, velocity field, and the potential written as $n_e(\mathbf{r}, t) = n_0 + n_{e1}(\mathbf{r}, t)$ ($|n_{e1}(\mathbf{r}, t)| \ll n_0$), $\mathbf{u}_e(\mathbf{r}, t) = \mathbf{u}_{e1}(\mathbf{r}, t)$, $\Phi(\mathbf{r}, z, t) = \Phi_1(\mathbf{r}, z, t)$, and $\bar{\Phi}(\mathbf{r}, 0, t) = \bar{\Phi}_1(\mathbf{r}, 0, t)$, where $n_{e1}(\mathbf{r}, t)$, $\mathbf{u}_{e1}(\mathbf{r}, t)$ and $\Phi_1(\mathbf{r}, z, t)$ represent the first-order perturbed values of the density, velocity, and potential. The linearized equations of the electronic excitation on the electron gas surface are obtained as follows:

$$\frac{\partial n_{e1}}{\partial t} + n_0 \nabla_{\parallel} \cdot \mathbf{u}_{e1} = 0, \quad (5)$$

$$\begin{aligned} m_e \frac{\partial \mathbf{u}_{e1}}{\partial t} &= e \nabla_{\parallel} \bar{\Phi}_1|_{z=0} - \frac{\pi\hbar^2}{m_e} \nabla_{\parallel} n_{e1} \\ &+ \frac{\hbar^2}{4m_e n_0} \nabla_{\parallel} (\nabla_{\parallel}^2 n_{e1}) \\ &- \gamma m_e \mathbf{u}_{e1} + m_e \eta \Delta_{\parallel} \mathbf{u}_{e1}, \end{aligned} \quad (6)$$

$$\nabla^2 \Phi_1 = 4\pi e [n_{e1} \delta(z) - Z_1 \delta(\mathbf{r} - \mathbf{v}t) \delta(z - z_0)]. \quad (7)$$

We adopt the time-space Fourier transform:

$$\frac{n_{e1}(\mathbf{r}, t)}{n_0} = A_n \int_{-\infty}^{+\infty} dq_y \int_{-\infty}^{+\infty} du \cdot \frac{q \cdot e^{-qz_0}}{|D_0|^2} \cos(\tilde{y}q_y) \quad (12)$$

$$\times \left[\text{Re}(D_0) \cos\left(\frac{\tilde{x}u}{\tilde{v}}\right) + \text{Im}(D_0) \sin\left(\frac{\tilde{x}u}{\tilde{v}}\right) \right],$$

$$\frac{\Phi_{\text{ind}}(\mathbf{r}, z, t)}{\Phi_n} = A_{\phi} \int_{-\infty}^{+\infty} dq_y \int_{-\infty}^{+\infty} du \cdot e^{-q \left(\frac{\tilde{z}_0 + \tilde{z}}{|D_0|^2 \cos(\tilde{y}q_y)} \left[\text{Re}(D_0) \cos\left(\frac{\tilde{x}u}{\tilde{v}}\right) + \text{Im}(D_0) \sin\left(\frac{\tilde{x}u}{\tilde{v}}\right) \right] \right)} \quad (13)$$

$$F(\mathbf{R}, t) = \iint \frac{d\mathbf{Q}d\omega}{(2\pi)^4} f(\mathbf{Q}, \omega) e^{i(\mathbf{Q}\cdot\mathbf{R} - \omega t)}, \quad (8)$$

where $F(\mathbf{R}, t)$ stands for any of the above-listed perturbed quantities, and $\mathbf{Q} = \{k_x, k_y, k_z\}$ is the wave vector. By using the Fourier transform in (5), (6), and (7), we can readily obtain the perturbed $n_{e1}(\mathbf{r}, t)$, the induced potential $\Phi_{\text{ind}}(\mathbf{r}, z, t)$, and the velocity field $\mathbf{u}_{e1}(\mathbf{r}, t)$ of perturbed electron gas:

$$n_{e1}(\mathbf{r}, t) = -n_0 \frac{Z_1 e^2}{2\pi m_e} \int d\mathbf{k} k e^{-kz_0} D^{-1}(k, \omega) e^{i\mathbf{k}\cdot(\mathbf{r}-\mathbf{v}t)}, \quad (9)$$

$$\Phi_{\text{ind}}(\mathbf{r}, z, t) = \frac{Z_1 e^3 n_0}{m_e} \int d\mathbf{k} e^{-k(z+z_0)} D^{-1}(k, \omega) e^{i\mathbf{k}\cdot(\mathbf{r}-\mathbf{v}t)}, \quad (10)$$

$$u_{e1x}(\mathbf{r}, t) = -\frac{Z_1 e^2}{2\pi m_e} \int d\mathbf{k} \cdot \frac{\omega}{k} \cdot \frac{k_x}{D(k, \omega)} \cdot e^{-kz_0} \cdot e^{i\mathbf{k}\cdot(\mathbf{r}-\mathbf{v}t)}, \quad (11a)$$

$$u_{e1y}(\mathbf{r}, t) = -\frac{Z_1 e^2}{2\pi m_e} \int d\mathbf{k} \cdot \frac{\omega}{k} \cdot \frac{k_y}{D(k, \omega)} \cdot e^{-kz_0} \cdot e^{i\mathbf{k}\cdot(\mathbf{r}-\mathbf{v}t)}, \quad (11b)$$

where $D(k, \omega) = ((\omega\tilde{\omega} - (kv_F)^2(1 + k^2/2k_F^2))/(2 - \omega_p^2(ka_B) + i\eta k^2 w))$, with $\tilde{\omega} = \omega + i\gamma$, Bohr radius $a_B = \hbar^2/m_e e^2$, Fermi velocity $v_F = \hbar k_F/m_e$, Fermi wave number $k_F = \sqrt{2\pi n_0}$, Fermi wave length $\lambda_f = 1/k_F$, electron plasma frequency $\omega_p = (2\pi n_0 e^2/m_e a_B)^{1/2}$, and the 2D wave vector $\mathbf{k} = \{k_x, k_y\}$. In addition, the direction of the projectile velocity \mathbf{v} is along with the x axis, for which $\omega = \mathbf{k} \cdot \mathbf{v}$, so that we can obtain $\omega = k_x v$.

For convenience, we introduce the dimensionless variables: $u = \omega/\omega_p$, $q_y = k_y/k_F$, $q = k/k_F$, $\tilde{v} = v/v_B$, $\tilde{l} = l/\lambda_f$, $\tilde{x} = ((x - vt)/\lambda_f)$, $\tilde{\gamma} = \gamma/\omega_p$, and $\tilde{\eta} = \eta/w_p/k_F^2$, where l stands for any quantity of length. By using the dimensionless variables above, (9), (10), (11a) and (11b) can be reduced to

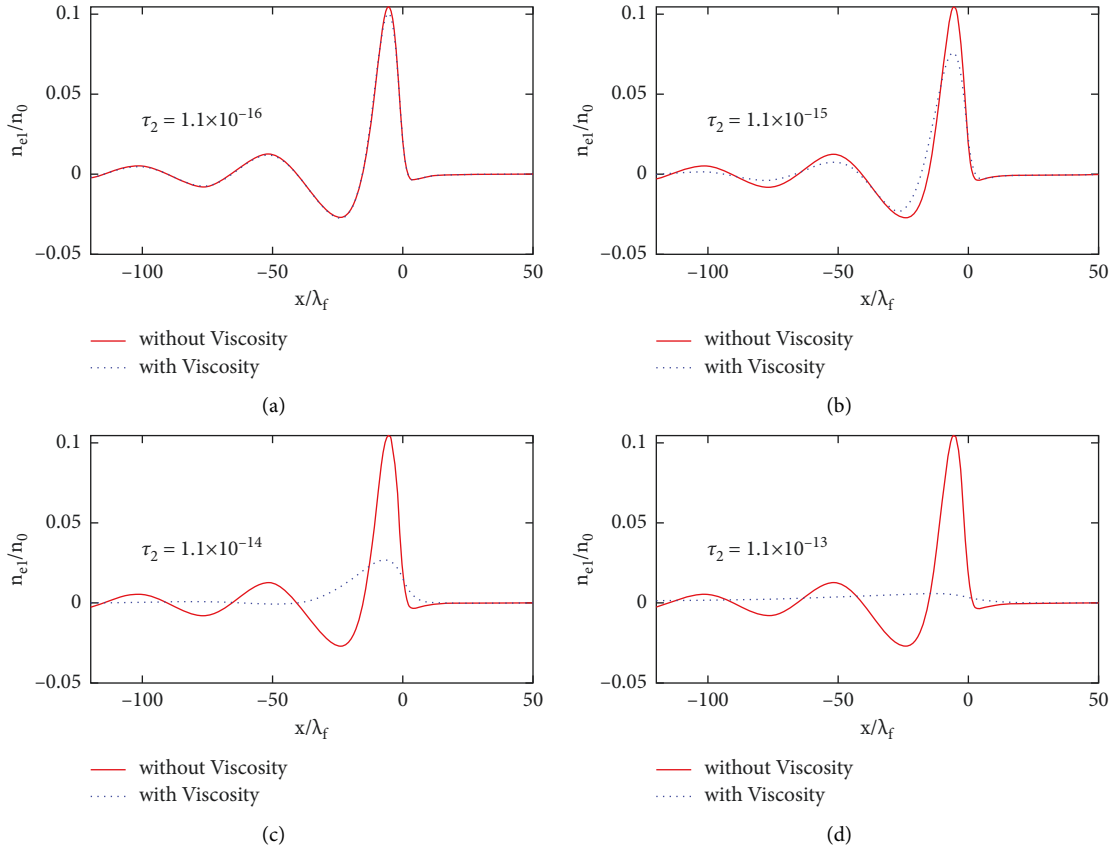


FIGURE 2: The perturbed electron gas density (normalized by n_0) with and without viscosity for different relaxation times τ_2 (i.e., different viscosity coefficients $\eta = (1/4)v_F^2\tau_2$ and the dimensionless variables $\bar{\eta} = \eta/w_p/k_F^2$): (a) $\tau_2 = 1.1 \times 10^{-16}$, (b) $\tau_2 = 1.1 \times 10^{-15}$, (c) $\tau_2 = 1.1 \times 10^{-14}$, and (d) $\tau_2 = 1.1 \times 10^{-13}$ with $r_s = 2$ and $\nu = 2\nu_B$.

$$\frac{u_{e1x}(\mathbf{r}, t)}{v_B} = A_{ux} \int_{-\infty}^{+\infty} dq_y \int_{-\infty}^{+\infty} du \cdot \frac{u^2 \cdot e^{-q\bar{z}}}{q \cdot |D_0|^2} \cos(\bar{y}q_y) \times \left[\text{Re}(D_0) \cos\left(\frac{\bar{x}u}{\bar{v}}\right) + \text{Im}(D_0) \sin\left(\frac{\bar{x}u}{\bar{v}}\right) \right], \quad (14a)$$

$$\frac{u_{e1y}(\mathbf{r}, t)}{v_B} = A_{uy} \int_{-\infty}^{+\infty} dq_y \int_{-\infty}^{+\infty} du \cdot \frac{u \cdot q_y \cdot e^{-q\bar{z}}}{q \cdot |D_0|^2} \sin(\bar{y}q_y) \times \left[\text{Re}(D_0) \sin\left(\frac{\bar{x}u}{\bar{v}}\right) - \text{Im}(D_0) \cos\left(\frac{\bar{x}u}{\bar{v}}\right) \right], \quad (14b)$$

where $A_n = (-Z_1)/2\pi r_s \bar{v}$, $A_\Phi = Z_1/2\pi \bar{v} r_s^2$, $\Phi_n = e/a_B$, $A_{ux} = ((-Z_1)/2\pi \bar{v}^2 r_s)$, and $A_{uy} = Z_1/2\pi \bar{v} r_s$, and

$$D_0(q, u) = u(u + i\bar{v}) - q^2 \left(\frac{(1 + (q^2/2))}{2r_s^2} \right) - \frac{q}{r_s} + iuq^2 \bar{\eta}, \quad (15)$$

is the dimensionless $D(k, \omega)$. Besides, $r_s = (2\pi n_0 a_B^2)^{-1/2}$ is the so-called Wigner radius as the function of density dependent on the material.

The stopping power $S(\nu) = -(dE/dx)$ originates from the induced potential:

$$S(\nu) = eZ_1 \frac{\partial \Phi_{\text{ind}}}{\partial x} \Big|_{z=z_0, \mathbf{r}=\mathbf{v}t}. \quad (16)$$

Thus, we can obtain the expression of the dimensionless stopping power:

$$\frac{S(\nu)}{S_0} = A_s \iint du dq_y e^{-2q\bar{z}_0} u \frac{I_m(D_0)}{|D_0|^2}, \quad (17)$$

where $A_s = Z_1^2/2\pi \bar{v} r_s^3$, $S_0 = (e/a_B)^2$. The form of dimensionless equations (12), (13), (14a), (14b), and (17) obtained above are similar to reference [64], but the internal forms are different, as reflected in the fact that the imaginary part of $D_0(q, u)$ takes into account the viscous effect $uq^2 \bar{\eta}$.

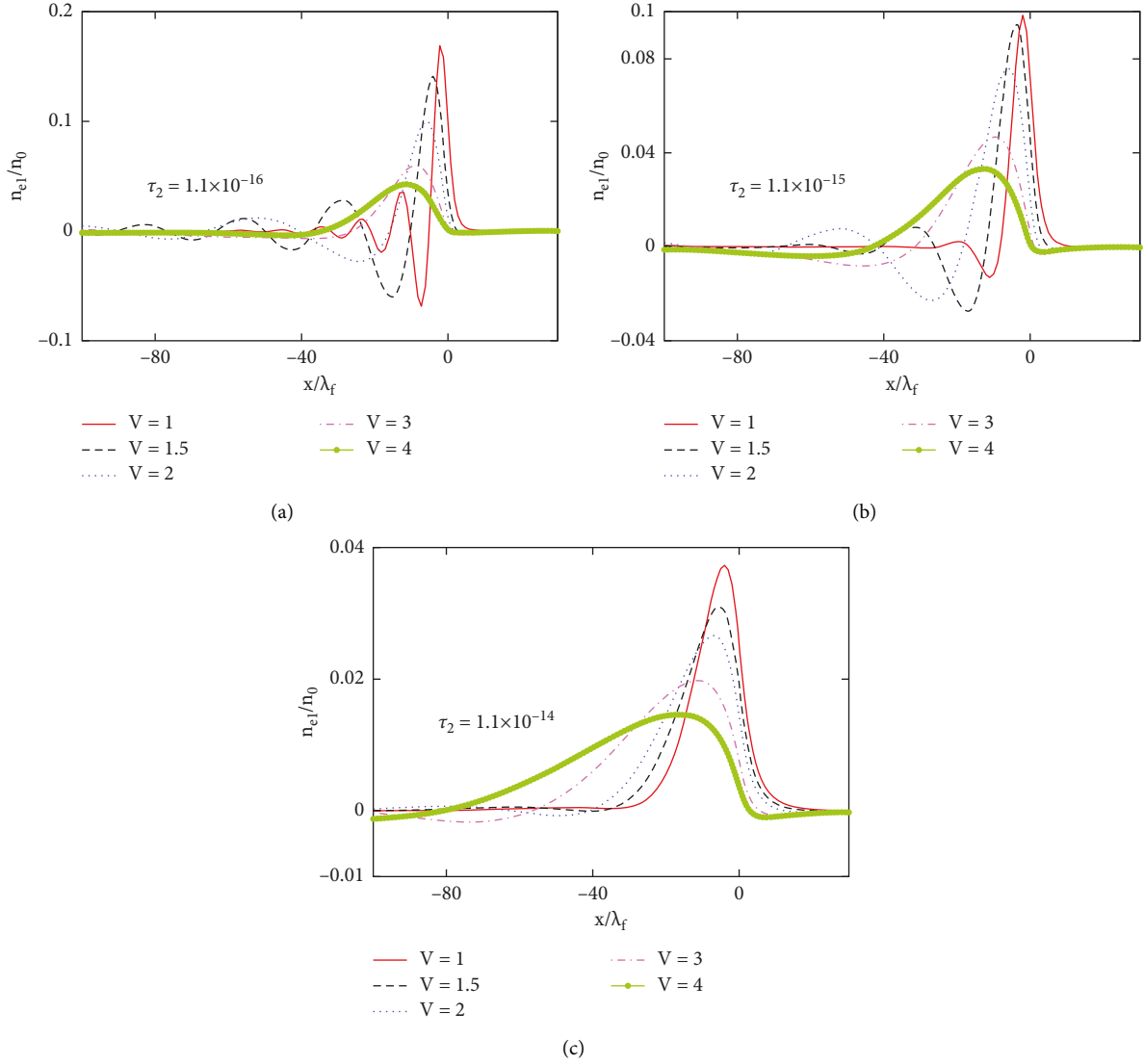


FIGURE 3: Comparisons of the perturbed electron gas density (normalized by n_0) in the different moving speeds of the incident particles in the case of considering different relaxation times τ_2 (i.e., different viscosity coefficients $\eta = (1/4)v_F^2\tau_2$ and the dimensionless variables $\bar{\eta} = \eta/\omega_p/k_F^2$): (a) $\tau_2 = 1.1 \times 10^{-16}$, (b) $\tau_2 = 1.1 \times 10^{-15}$, and (c) $\tau_2 = 1.1 \times 10^{-14}$ with $r_s = 2$.

In the next section, the results of the perturbed electrons gas density, the velocity vector field of the perturbed electron gas, and the stopping power are obtained numerically according to (12), (14a), (14b), and (17), respectively, where the MATLAB solver function (integral2 function) is used to solve the double integral. Referring to [64] for parameter selection, we take the charge number of the incident particle is a proton $Z_1 = 1$, the friction coefficient $\gamma = 0.02\omega_p$, the height $z_0 = 3.0\lambda_f$, and $r_s = 2$ kept fixed throughout the study. The QHD method is suitable to calculate the stopping power for higher particle velocities greater than the Bohr velocity, as discussed in our previous work [69]. Thus, for the velocity of the incident particle, we start from $v = v_B$.

3. Numerical Results

3.1. The Perturbed Electron Density. We have solved (12) numerically for the values of the plasma configuration

parameters $v = 2v_B$ and $r_s = 2$ in the case of with and without viscosity. The results are shown in Figure 2, showing the distribution of perturbed electron gas density n_{e1} (normalized by n_0). Then, how the perturbed density of the electron gas is impacted by viscosity will be discussed. Equation (1) shows that the viscosity coefficient η is a function of the relaxation time τ_2 , linearly increasing as τ_2 increases. To examine the effects of the viscosity on the perturbation of the electron gas, we plot Figure 2 for four relaxation time values ($\tau_2 = 1.1 \times 10^{-16}$, 1.1×10^{-15} , 1.1×10^{-14} , and 1.1×10^{-13}) with $r_s = 2$ and $v = 2v_B$. Note that, as τ_2 increases (namely, η increases), the oscillation amplitudes of the perturbed density decrease, and then, finally, the peak is suppressed and disappears gradually. We can also see in Figure 2 that the perturbed region becomes smaller when τ_2 increases. This is because when the incident particles move above 2DEG, part energy of the incident particles is dissipated by the viscous effect, leading to a

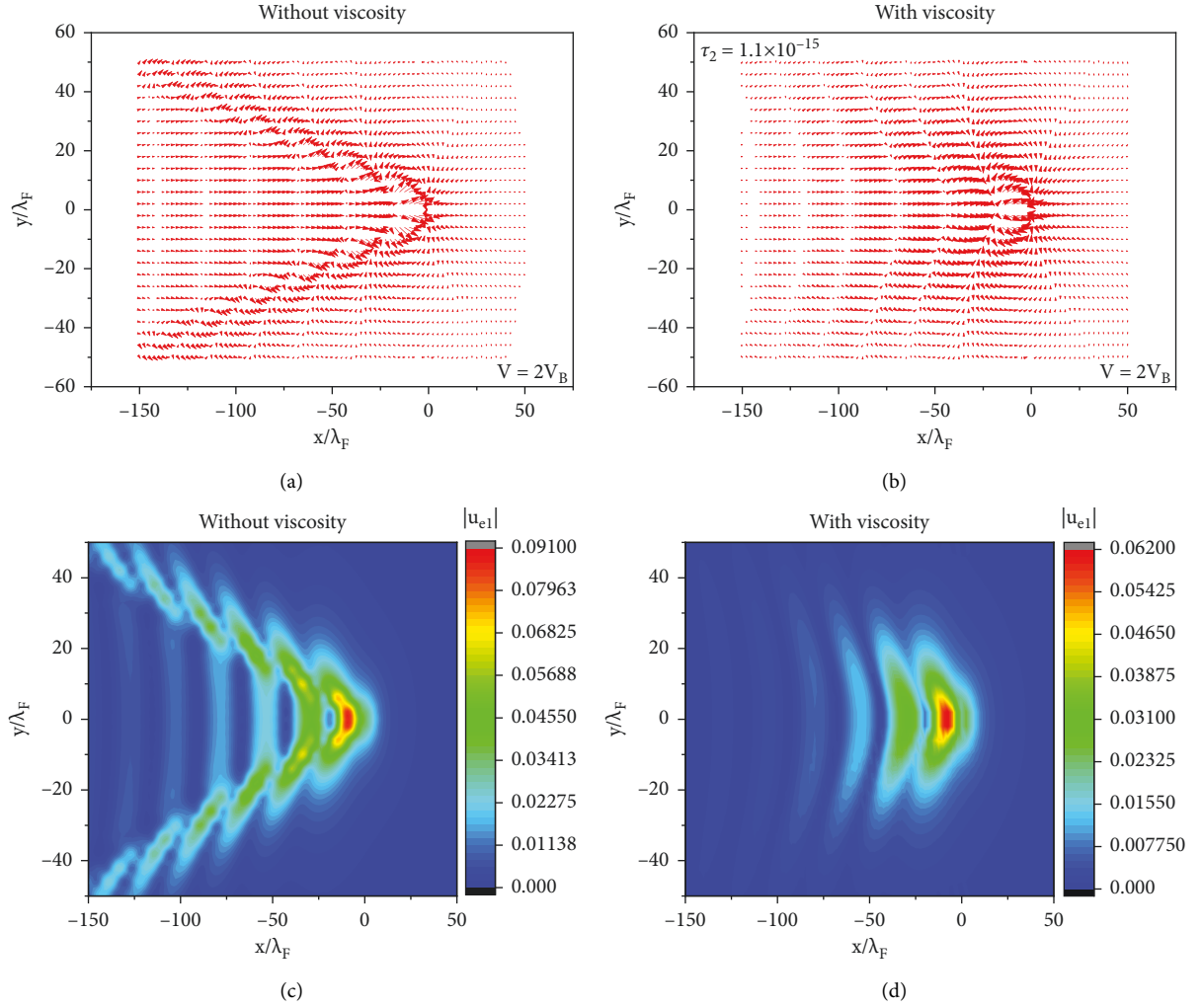


FIGURE 4: The spatial distribution and magnitude of the velocity vector field (normalized by v_B): (a) the spatial distribution of the velocity vector field without viscosity, (b) the spatial distribution of the velocity vector field with viscosity, (c) the magnitude of the velocity vector field without viscosity, and (d) the magnitude of the velocity vector field with viscosity, where $v = 2v_B$, $r_s = 2$, and $\tau_2 = 1.1 \times 10^{-15}$.

decrease in the energy that makes the electron gas movement. It can be clearly seen that electron density perturbation is significantly suppressed at high viscosity.

The comparison of the perturbed electron gas density for the different moving speeds ($v = v_B$, $v = 1.5v_B$, $v = 2v_B$, $v = 3v_B$, and $v = 4v_B$) is shown in Figure 3 with three relaxation time values ($\tau_2 = 1.1 \times 10^{-16}$, 1.1×10^{-15} , and 1.1×10^{-14}). In the case of low viscosity shown in Figure 3(a), one can find that the curves of the perturbed electron gas density demonstrate an obvious difference for spatial change, which indicates that the projectile speed has a strong influence on the wake-field. The number of wake-field oscillations excited behind the incident particles decreases with increasing velocity. The maximum values decrease in magnitude with the increasing v , and its position shifts toward lower values. The trend of this change shows good agreement with the conclusion in reference [45], which also showed the decrease in the maximum values and the number of wake-field oscillations. Figures 3(b) and 3(c) show the

curves of the perturbed electron gas density for different viscosities with $\tau_2 = 1.1 \times 10^{-15}$ and 1.1×10^{-14} , showing similar change tendencies with those in Figure 3(a) for fixed τ_2 . However, as shown in Figures 3(b) and 3(c), an interesting phenomenon appears when the incident particle moves along x direction with a certain speed in different values of the viscosity, in which the strength of the perturbed electron gas density decreases and the perturbed region become smaller as viscosity increases, which is in agreement with that shown in Figure 2. At a fixed incident particle velocity, the curve exhibits multiple wake-field oscillations behind the particle with low viscosity, while the oscillations vanish with high viscosity.

3.2. The Spatial Distribution of the Velocity Vector Field. Figures 4 and 5 show the spatial distribution of the velocity vector field of perturbed electron gas for different incident particle speeds to further understand the influence of

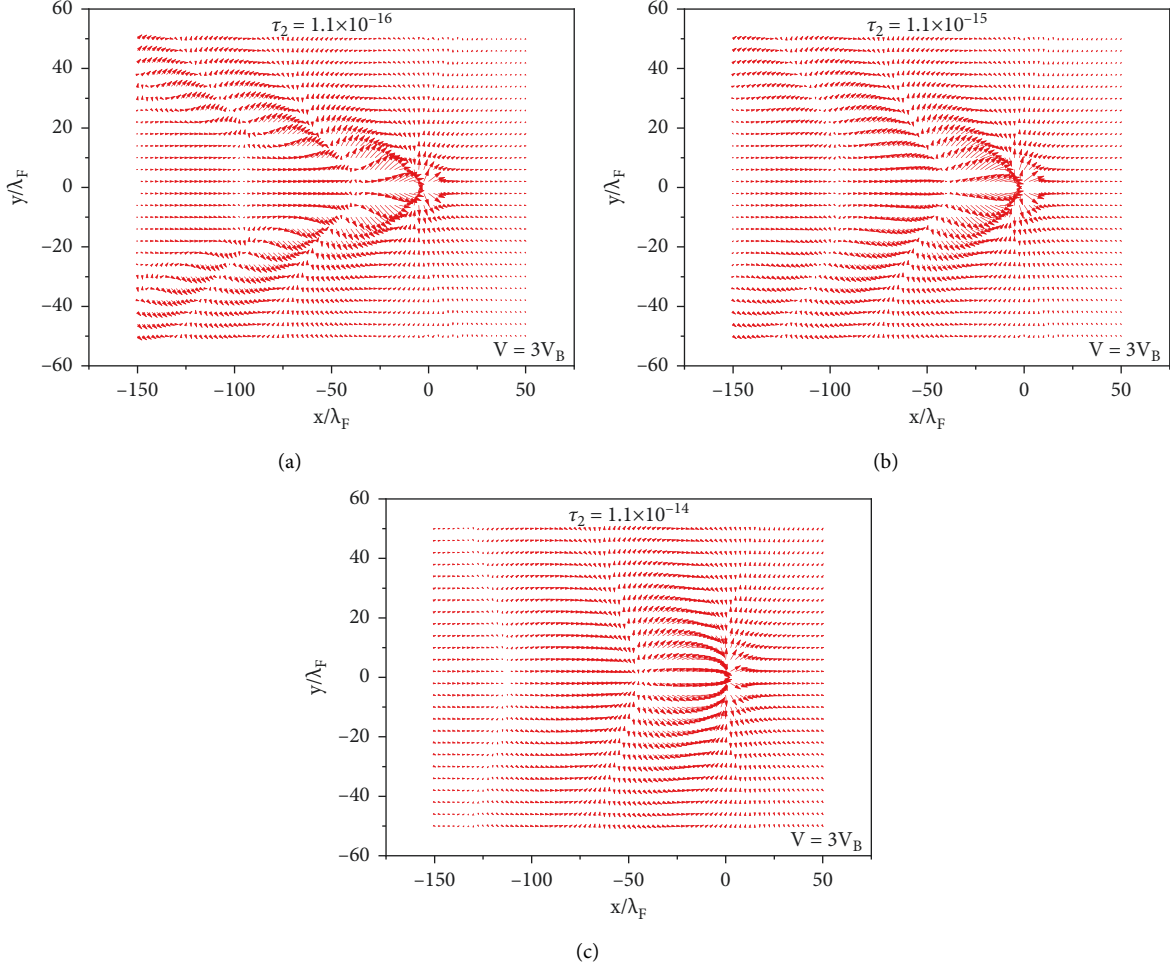


FIGURE 5: The spatial distribution of the velocity vector field of perturbed electron gas \mathbf{u}_{e1} (normalized by v_B) in the case of viscosity for different relaxation times (i.e., different viscosity coefficients $\eta = (1/4)v_F^2\tau_2$ and the dimensionless variables $\bar{\eta} = \eta/w_p/k_F^2$): $\tau_2 =$ (a) 1.1×10^{-16} , (b) 1.1×10^{-15} , and (c) 1.1×10^{-14} , with $v = 3v_B$.

viscosity. We first show in Figures 4(a) and 4(b) the spatial distribution of the velocity vector field with $v = 2v_B$, $r_s = 2$, and $\tau_2 = 1.1 \times 10^{-15}$. One can see from Figures 4(a) and 4(b) that the wake-field is almost axially symmetric about the y axis, compared with those in the case of considering the viscosity shown in Figure 4(b), in which the V-shaped cones structures lag slightly behind the incident particles, along with fewer oscillatory lateral wakes. Besides, we also observe that these structures are composed of multiple cones, which become fewer in consideration of the viscosity. However, the magnitude of the velocity vector field $|\mathbf{u}_{e1}|$ can be also determined by the viscosity, which can be inferred from (14a) and (14b) in the imaginary part of D_0 . Thus, the magnitude of the velocity field of the electrons $|\mathbf{u}_{e1}|$ in the wake-field region is shown in Figures 4(c) and 4(d). The main features observed in Figures 4(a) and 4(b) are shown in Figures 4(c) and 4(d). Moreover, the maximum value of $|\mathbf{u}_{e1}|$ is suppressed when the viscosity is taken into account, indicating the viscosity makes the electron gas more difficult to be disturbed. These characteristics closely resemble the spatial distribution of perturbed electron gas density n_{e1} .

As demonstrated above, viscosity affects the spatial distribution and affects the maximum value of the velocity vector field. Thus, such a viscosity effect on the velocity vector of the perturbed electron gas \mathbf{u}_{e1} is shown in Figures 5(a)–5(c) with viscosity for different relaxation times $\tau_2 = 1.1 \times 10^{-16}$, $\tau_2 = 1.1 \times 10^{-15}$, and $\tau_2 = 1.1 \times 10^{-14}$ with $v = 3v_B$. From Figure 5(a), we can see that in the low-viscosity case ($\tau_2 = 1.1 \times 10^{-16}$), the characteristics closely resemble the case of without considering the viscosity in Figure 4(a). The similar cone structures of the velocity field and invariably symmetrical spatial distributions concerning the y axis are still reproduced in the wake-field regions, showing the evident dynamic polarization of the perturbed electron gas. The same pattern has also been found in reference [19], in which the dynamic polarization of perturbed electrons becomes obvious with increasing magnetic field. However, as shown in Figures 5(b) and 5(c) with the increasing viscosity, the opening cone angles of the V-shaped wake-field decrease, and the oscillation tails disappear gradually, showing the wakening of the dynamic polarization, which is completely different from the velocity

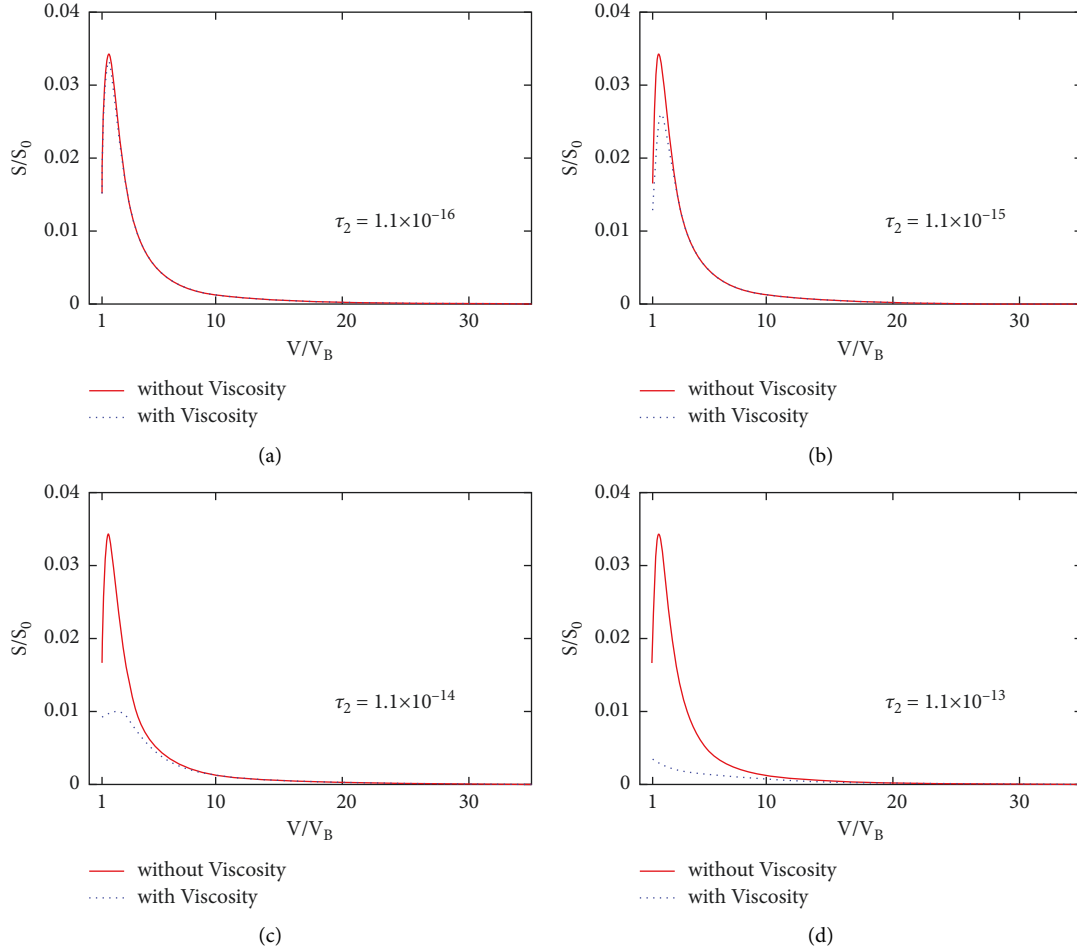


FIGURE 6: The stopping power S (normalized by $S_0 = (e/a_B)^2$) versus the moving speed with and without viscosity for different relaxation times τ_2 (i.e., different viscosity coefficients η and the dimensionless variables $\bar{\eta} = \eta/w_p/k_F^2$): (a) $\tau_2 = 1.1 \times 10^{-16}$, (b) $\tau_2 = 1.1 \times 10^{-15}$, (c) $\tau_2 = 1.1 \times 10^{-14}$, and (d) $\tau_2 = 1.1 \times 10^{-13}$ with $r_s = 2$.

distribution under the influence of magnetic field that the dynamic polarization is enhanced as the magnetic field increases [19]. It can be concluded that the movement of the perturbed electron gas is increasingly restricted under the influence of viscosity. In this case, the electrons cannot fully respond to the disturbance from the incident particles, giving rise to the reduction in the wake region.

3.3. Stopping Power. The viscosity significantly impacts the density and velocity vector field of the perturbed electron gas. As a result, such an influence can also be seen in the stopping power, as shown in Figure 6, showing how the electronic stopping character is impacted by viscosity. The influence of viscosity is reflected clearly in Figure 6 where the stopping power is plotted as a function of velocity for the same condition shown in Figure 2. The main features observed in the perturbed density are reproduced in the stopping power. With the increasing τ_2 values shown in Figure 6, at the high-velocity region, the two curves for the stopping power show agreement with each other, while at the low-velocity region, the peak values of the stopping

power get weaker, showing less energy loss from projectiles. Besides, note that the peak position of the stopping power shifts mainly to the lower-velocity region with the viscosity. Finally, the peak is limited to become a broad plateau, indicating that the energy loss of the particle is hardly influenced by the viscosity when the viscosity reaches a considerable value. The above results are entirely different from those in reference [19], in which the significant enhancement of the stopping power has been observed with the increasing magnetic field. Therefore, one can expect that the differences of the results between the two situations of with and without viscosity are due to the action of the viscosity on the perturbed electron gas density and velocity vector field in the plane at their distribution and magnitude, which can be seen in parts of the perturbed electron density and the spatial distribution of the velocity vector field.

4. Summary

The purpose of this study was first to derive a self-consistent quantum hydrodynamic model that incorporates quantum and viscosity effects. Then, two-dimensional simulations are

performed to investigate the interaction of the moving charged particle with 2DQEG, taking into account the viscosity based on the QHD model. Special attention is paid to the influences of the viscosity during interaction. The analytical expressions of the perturbed electron density, the velocity vector field in 2DQEG, and the stopping power have been derived based on the assumption of the linear disturbance. Results show that the viscosity effect suppresses the perturbation of the electron gas density and velocity vector field in the two-dimensional plane. As for considering the viscosity effect, our simulation results show that the oscillatory behaviors of the perturbed density and velocity vector field turn up in the case of small viscosity and then disappear gradually with the increasing of the viscosity. Besides, the magnitude of the wake-field decreases, and the perturbed regions caused by the moving particles get smaller due to the restriction on electron motion as the viscosity increases. The same trend is reproduced as the velocity of the incident particle increases. Furthermore, the perturbed density may change locally without changing in the surroundings due to the action of the viscous term [70]. The results indicate that the wake-field oscillation amplitude will decrease, and the incident particle will suffer less energy loss as the viscosity has been taken into account. Furthermore, in the stopping power calculation, the charged particle will suffer less energy loss.

In conclusion, viscosity not only affects the spatial distribution but also affects the magnitude. This is because the existence of the viscous term makes the electron gas less likely to be disturbed, resulting in the weakening of the electron polarization. In other words, due to the presence of a viscous effect, the average flow velocity of the electron gas is reduced, and the viscous flows may show a peculiar behavior that self-organizes into streams with different speeds. As a result, the distribution and magnitude of the disturbing electron gas are changed, giving rise to the reduction in the stopping power.

In summary, the model proposed in this study can be used in any system with two-dimensional electron gas such as the two-dimensional monovalent layered metal PdCoO₂ [67], graphene [52], and the GaAs quantum wells [55]. What is more, viscosity term is a key quantity in the hydrodynamic regime, which could change the interaction mechanism of ions and a quantum 2DEG, such a 2DEG can be performed in various modern developments in the field of semiconductor heterostructures [71], nanoscale objects such as nanowires, quantum dot, the metal surface at the nanoscale [47], and graphene [72]. The viscosity in 2D electron fluid can offer a promising opportunity to use various scanning probes to estimate the stopping power for surface detecting. Likewise, we can also estimate viscosity by measuring the stopping power. Furthermore, hydrodynamic characteristics, i.e., the viscosity of the 2D electron fluid, can be particularly enhanced by tuning the configuration or doping of the samples to change the electron gas density to achieve the purpose of stopping power modulation. Furthermore, the viscous effects can promote high mobility transmission at elevated temperatures, which is a potentially useful behavior for designing graphene-based devices [73]. Consequently,

for our future study, we would like to extend the present work on the presence of external magnetic fields under high temperatures.

Data Availability

The data used to support the findings of this study are available from the corresponding author upon request.

Conflicts of Interest

The authors declare that they have no conflicts of interest.

Acknowledgments

This work was supported by the National Key R&D Program of China (2017YFE0301801), the National Natural Science Foundation of China (11975174 and 11775090), and the Fundamental Research Funds for the Central Universities (WUT: 2020IB023 and 2018IB011).

References

- [1] P. M. Echenique, F. Flores, and R. H. Ritchie, "Dynamic screening of ions in condensed matter," *Solid State Physics*, vol. 43, 1990.
- [2] T. J. Gramila, J. P. Eisenstein, A. H. MacDonald, L. N. Pfeiffer, and K. W. West, "Electron-electron scattering between parallel two-dimensional electron gases," *Surface Science*, vol. 263, no. 1-3, pp. 446-450, 1992.
- [3] A. G. Borisov, J. Ji, R. D. Muiño, D. Sánchez-Portal, and P. M. Echenique, "Quantum-size effects in the energy loss of charged particles interacting with a confined two-dimensional electron gas," *Physical Review*, vol. 73, no. 1, Article ID 012901, 2006.
- [4] I. Radović and D. Borka, "Interactions of fast charged particles with supported two-dimensional electron gas: one-fluid model," *Physics Letters A*, vol. 374, no. 13, pp. 1527-1533, 2010.
- [5] C.-Z. Li, S.-R. Na, Y.-Y. Jian, Y.-N. Wang, and Z. L. Mišković, "Interactions of the external charged particle beams with double-layer two-dimensional electron gases separated by insulating medium," *Radiation Effects and Defects in Solids*, vol. 174, no. 1, pp. 19-30, 2019.
- [6] S. G. Elkomoss and A. Pape, "Stopping-power calculations for semiconductors," *Physical Review B*, vol. 26, no. 12, pp. 6739-6746, 1982.
- [7] J. Jacoby, D. H. H. Hoffmann, W. Laux et al., "Stopping of heavy ions in a hydrogen plasma," *Physical Review Letters*, vol. 74, no. 9, pp. 1550-1553, 1995.
- [8] Y. Zhang, W. Jiang, and L. Yi, "Stopping power of two-dimensional spin quantum electron gases," *Nuclear Instruments and Methods in Physics Research Section B: Beam Interactions with Materials and Atoms*, vol. 349, pp. 72-78, 2015.
- [9] W. Cayzac, A. Frank, A. Ortner et al., "Experimental discrimination of ion stopping models near the Bragg peak in highly ionized matter," *Nature Communications*, vol. 8, no. 1, Article ID 15693, 2017.
- [10] C. Deutsch, G. Maynard, M. Chabot, D. Gardes, and S. Della-Negra, "Ion stopping in dense plasma target for high energy density physics," *Open Plasma Physics Journal*, vol. 3, no. 1, 2010.

- [11] J. Ren, Z. Deng, W. Qi et al., "Observation of a high degree of stopping for laser-accelerated intense proton beams in dense ionized matter," *Nature Communications*, vol. 11, no. 1, p. 5157, 2020.
- [12] A. B. Zylstra, J. A. Frenje, P. E. Grabowski et al., "Measurement of charged-particle stopping in warm dense plasma," *Physical Review Letters*, vol. 114, no. 21, Article ID 215002, 2015.
- [13] Y. T. Zhao, Y. N. Zhang, R. Cheng et al., "Benchmark experiment to prove the role of projectile excited states upon the ion stopping in plasmas," *Physical Review Letters*, vol. 126, no. 11, Article ID 115001, 2021.
- [14] M. Nastasi, J. W. Mayer, and Y. Wang, *Ion Beam Analysis: Fundamentals and Applications*, CRC Press, Boca Raton, FL, USA, 2014.
- [15] A. Ghicov, J. M. Macak, H. Tsuchiya et al., "Ion implantation and annealing for an efficient N-doping of TiO₂ nanotubes," *Nano Letters*, vol. 6, no. 5, pp. 1080–1082, 2006.
- [16] H. Zhang, F. W. Meyer, H. M. Meyer III, and M. J. Lance, "Surface modification and chemical sputtering of graphite induced by low-energy atomic and molecular deuterium ions," *Vacuum*, vol. 82, no. 11, pp. 1285–1290, 2008.
- [17] C.-W. Lee and A. Schleife, "Hot-electron-mediated ion diffusion in semiconductors for ion-beam nanostructuring," *Nano Letters*, vol. 19, no. 6, pp. 3939–3947, 2019.
- [18] A. A. Correa, "Calculating electronic stopping power in materials from first principles," *Computational Materials Science*, vol. 150, pp. 291–303, 2018.
- [19] Z. H. Hu, Y. H. Song, Y.-H. Hu, and Y. N. Wang, "Wake effect and stopping power for a charged ion moving in magnetized two-component plasmas: two-dimensional particle-in-cell simulation," *Physical Review*, vol. 82, no. 2, Article ID 026404, 2010.
- [20] P. Haussalo, K. Nordlund, and J. Keinonen, "Stopping of 5–100 keV helium in tantalum, niobium, tungsten, and AISI 316L steel," *Nuclear Instruments and Methods in Physics Research Section B: Beam Interactions with Materials and Atoms*, vol. 111, pp. 1–2, 1996.
- [21] Y. Zhang, G. M. Stocks, K. Jin et al., "Influence of chemical disorder on energy dissipation and defect evolution in concentrated solid solution alloys," *Nature Communications*, vol. 6, no. 1, p. 8736, 2015.
- [22] Y. Zhang and W. Jiang, "Pseudomagnetic field modulation of stopping power for a charged particle moving above graphene," *Physics of Plasmas*, vol. 25, no. 7, Article ID 072107, 2018.
- [23] Y. V. Bulgakov, V. S. Nikolaev, and V. I. Shulga, "The experimental determination of the impact parameter dependence of inelastic energy loss of channeled ions," *Physics Letters A*, vol. 46, no. 7, pp. 477–478, 1974.
- [24] Ya. Zhang, Y.-H. Song, and Y.-N. Wang, "Study of stopping power for a proton moving in a plasma with arbitrary degeneracy," *Physics of Plasmas*, vol. 20, no. 10, Article ID 102121, 2013.
- [25] N. Hünemohr, B. Krauss, C. Tremmel, B. Ackermann, O. Jäkel, and S. Greulich, "Experimental verification of ion stopping power prediction from dual energy CT data in tissue surrogates," *Physics in Medicine and Biology*, vol. 59, no. 1, 2013.
- [26] S. Kalbitzer, H. Oetzmann, H. Grahmann, and A. Feuerstein, "A simple universal fit formula to experimental nuclear stopping power data," *Zeitschrift für Physik A: Atoms and Nuclei*, vol. 278, no. 3, pp. 223–224, 1976.
- [27] H. Paul, "A comparison of recent stopping power tables for light and medium-heavy ions with experimental data, and applications to radiotherapy dosimetry," *Nuclear Instruments and Methods in Physics Research Section B: Beam Interactions with Materials and Atoms*, vol. 247, no. 2, 172 pages, 2006.
- [28] N. J. M. Horing, H. C. Tso, and G. Gumbs, "Fast-particle energy loss in the vicinity of a two-dimensional plasma," *Physical Review B*, vol. 36, no. 3, pp. 1588–1594, 1987.
- [29] G. Zwicknagel, C. Toepffer, and P.-G. Reinhard, "Stopping of heavy ions in plasmas at strong coupling," *Physics Reports*, vol. 309, no. 3, pp. 117–208, 1999.
- [30] H. B. Nersisyan, G. Zwicknagel, and C. Toepffer, "Energy loss of ions in a magnetized plasma: conformity between linear response and binary collision treatments," *Physical review. E, Statistical, nonlinear, and soft matter physics*, vol. 67, no. 2, Article ID 026411, 2003.
- [31] S. Ali and P. K. Shukla, "Potential distributions around a moving test charge in quantum plasmas," *Physics of Plasmas*, vol. 13, no. 10, Article ID 102112, 2006.
- [32] A. Krakovsky and J. K. Percus, "Nonlinear calculation of the stopping power of a two-dimensional electron gas for heavy particles," *Physical Review. B, Condensed Matter*, vol. 52, no. 4, pp. R2305–R2308, 1995.
- [33] I. Nagy, J. László, and J. Giber, "Dynamic local field correction in the calculation of electronic stopping power," *Zeitschrift für Physik A Atoms and Nuclei*, vol. 321, no. 2, pp. 221–223, 1985.
- [34] I. Nagy, J. László, and J. Giber, "Local-field corrections in the calculation of electronic stopping power for protons," *Nuclear Instruments and Methods in Physics Research Section B: Beam Interactions with Materials and Atoms*, vol. 12, no. 1, pp. 34–37, 1985.
- [35] E. Zaremba, I. Nagy, and P. M. Echenique, "Nonlinear screening and stopping power in two-dimensional electron gases," *Physical Review B*, vol. 71, no. 12, Article ID 125323, 2005.
- [36] P. M. Echenique and M. E. Uranga, "Density functional theory of stopping power," *Interaction of Charged Particles with Solids and Surfaces*, Springer, Berlin, Germany, 1991.
- [37] G. Zwicknagel, C. Toepffer, and P.-G. Reinhard, "Molecular dynamic simulations of ions in electron plasmas at strong coupling," *Hyperfine Interactions*, vol. 99, no. 1, pp. 285–291, 1996.
- [38] G. Zwicknagel, "Nonlinear energy loss of heavy ions in plasma," *Nuclear Instruments and Methods in Physics Research Section B Beam Interactions with Materials and Atoms*, vol. 197, no. 1–2, pp. 22–38, 2002.
- [39] A. J. Bennett and J. Alan, "Influence of the electron charge distribution on surface-plasmon dispersion," *Physical Review B*, vol. 1, no. 1, pp. 203–207, 1970.
- [40] M. Marklund, G. Brodin, L. Stenflo, and C. S. Liu, "New quantum limits in plasmonic devices," *EPL (Europhysics Letters)*, vol. 84, no. 1, pp. 17006–17551, 2008.
- [41] X. Chen, H. R. Park, M. Pelton et al., "Atomic layer lithography of wafer-scale nanogap arrays for extreme confinement of electromagnetic waves," *Nature Communications*, vol. 4, p. 2361, 2013.
- [42] X. Chen, C. Ciraci, David R. Smith, and S.-H. Oh, "Nanogap-enhanced infrared spectroscopy with template-stripped wafer-scale Arrays of buried plasmonic cavities," *Nano Letters*, vol. 15, no. 1, pp. 107–113, 2015.
- [43] G. Manfredi and F. Haas, "Self-consistent fluid model for a quantum electron gas," *Physical Review B*, vol. 64, no. 7, Article ID 075316, 2001.

- [44] F. Haas, G. Manfredi, and M. Feix, "Multistream model for quantum plasmas," *Physical Review*, vol. 62, no. 2, pp. 2763–2772, 2000.
- [45] C.-Z. Li, Y.-H. Song, and Y.-N. Wang, "Wake effects and energy loss for a charged particle moving above a thin metal film," *Physical Review*, vol. 79, no. 6, Article ID 062903, 2009.
- [46] C.-Z. Li, Y.-H. Song, and Y.-N. Wang, "Energy loss of a charged particle moving outside a nano-dielectric sphere covered with infinitesimally thin metal film," *Nuclear Instruments and Methods in Physics Research Section B: Beam Interactions with Materials and Atoms*, vol. 267, no. 18, pp. 3129–3132, 2009.
- [47] Y. Zhang, M. X. Gao, and B. Guo, "Surface plasmon dispersion relation at an interface between thin metal film and dielectric using a quantum hydrodynamic model," *Optics Communications*, vol. 402, pp. 326–329, 2017.
- [48] Ya. Zhang, F. Zhai, B. Guo, Yi Lin, and W. Jiang, "Quantum hydrodynamic modeling of edge modes in chiral Berry plasmons," *Physical Review B*, vol. 96, no. 4, Article ID 045104, 2017.
- [49] Ya. Zhang, F. Zhai, and W. Jiang, "Effect of Stern-Gerlach force on negative magnetoresistance and Hall resistance in spin-dependent viscous flow," *Physical Review B*, vol. 102, no. 4, Article ID 045133, 2020.
- [50] J. Gooth, F. Menges, N. Kumar et al., "Thermal and electrical signatures of a hydrodynamic electron fluid in tungsten diphosphide," *Nature Communications*, vol. 9, no. 1, p. 4093, 2018 1–8.
- [51] A. D. Levin, G. M. Gusev, E. V. Levinson, Z. D. Kvon, and A. K. Bakarov, "Vorticity-induced negative nonlocal resistance in a viscous two-dimensional electron system," *Physical Review B*, vol. 97, no. 24, Article ID 245308, 2018.
- [52] D. A. Bandurin, I. Torre, R. Krishna Kumar et al., "Negative local resistance caused by viscous electron backflow in graphene," *Science*, vol. 351, no. 6277, pp. 1055–1058, 2016.
- [53] G. M. Gusev, A. D. Levin, E. V. Levinson, and A. K. Bakarov, "Viscous electron flow in mesoscopic two-dimensional electron gas," *AIP Advances*, vol. 8, no. 2, Article ID 025318, 2018.
- [54] G. M. Gusev, A. S. Jaroshevich, A. D. Levin, Z. D. Kvon, and A. K. Bakarov, "Stokes flow around an obstacle in viscous two-dimensional electron liquid," *Scientific Reports*, vol. 10, no. 1, pp. 1–9, 2020.
- [55] P. S. Alekseev, "Negative magnetoresistance in viscous flow of two-dimensional electrons," *Physical Review Letters*, vol. 117, no. 16, Article ID 166601, 2016.
- [56] R. Cohen and M. Goldstein, "Hall and dissipative viscosity effects on edge magnetoplasmons," *Physical Review B*, vol. 98, no. 23, Article ID 235103, 2018.
- [57] P. S. Alekseev, "Magnetic resonance in a high-frequency flow of a two-dimensional viscous electron fluid," *Physical Review B*, vol. 98, no. 16, Article ID 165440, 2018.
- [58] P. S. Alekseev and A. P. Alekseeva, "Transverse magnetosonic waves and viscoelastic resonance in a two-dimensional highly viscous electron fluid," *Physical Review Letters*, vol. 123, no. 23, Article ID 236801, 2019.
- [59] A. Jünger and S. Tang, "Numerical approximation of the viscous quantum hydrodynamic model for semiconductors," *Applied Numerical Mathematics*, vol. 56, no. 7, pp. 899–915, 2006.
- [60] M. P. Gualdini and A. Jünger, "Analysis of the viscous quantum hydrodynamic equations for semiconductors," *European Journal of Applied Mathematics*, vol. 15, no. 5, pp. 577–595, 2004.
- [61] T. Ahmed, A. Rehman, A. Ali, and S. Qamar, "A high order multi-resolution WENO numerical scheme for solving viscous quantum hydrodynamic model for semiconductor devices," *Results in Physics*, vol. 23, Article ID 104078, 2021.
- [62] S. Rudin, "Viscous hydrodynamic model of non-linear plasma oscillations in two-dimensional conduction channels and application to the detection of terahertz signals," *Optical and Quantum Electronics*, vol. 42, no. 11–13, pp. 793–799, 2011.
- [63] P. Sharma and R. K. Chhajlani, "Effect of spin-induced magnetization and Hall current on self-gravitational instability of magnetized viscous quantum plasma," *Journal of Plasma Physics*, vol. 81, no. 2, Article ID 905810208, 2014.
- [64] C.-Z. Li, Y.-H. Song, and Y.-N. Wang, "Wake effects and stopping power for a charged particle moving above two-dimensional quantum electron gases," *Physics Letters A*, vol. 372, no. 24, pp. 4500–4504, 2008.
- [65] L. D. Landau and E. M. Lifshitz, *Fluid Mechanics*, Elsevier, Amsterdam, Netherlands, 2nd edition, 1959.
- [66] P. S. Alekseev and A. P. Dmitriev, "Viscosity of two-dimensional electrons," *Physical Review B*, vol. 102, no. 24, Article ID 241409, 2020.
- [67] P. J. W. Moll, P. Kushwaha, N. Nandi, B. Schmidt, and A. P. Mackenzie, "Evidence for hydrodynamic electron flow in PdCoO₂," *Science*, vol. 351, no. 6277, pp. 1061–1064, 2016.
- [68] D. Liang, T. Wei, J. Wang, and J. Li, "Quasi van der Waals epitaxy nitride materials and devices on two dimension materials," *Nano Energy*, vol. 69, Article ID 104463, 2020.
- [69] Y. Zhang, Y.-H. Song, and Y.-N. Wang, "Stopping power for a charged particle moving through three-dimensional nonideal finite-temperature electron gases," *Physics of Plasmas*, vol. 18, no. 7, Article ID 072701, 2011.
- [70] J. C. Dyre, "Solidity of viscous liquids. IV. Density fluctuations," *Physical review. E, Statistical, nonlinear, and soft matter physics*, vol. 74, no. 2, Article ID 021502, 2006.
- [71] T.-H. Hung, M. Esposito, and S. Rajan, "Interfacial charge effects on electron transport in III-nitride metal insulator semiconductor transistors," *Applied Physics Letters*, vol. 99, no. 16, Article ID 162104, 2011.
- [72] S. A. Mikhailov, "Theory of the giant plasmon-enhanced second-harmonic generation in graphene and semiconductor two-dimensional electron systems," *Physical Review B*, vol. 84, no. 4, Article ID 045432, 2011.
- [73] R. Krishna Kumar, D. A. Bandurin, F. M. D. Pellegrino et al., "Superballistic flow of viscous electron fluid through graphene constrictions," *Nature Physics*, vol. 13, no. 12, pp. 1182–1185, 2017.